Antarct. Meteorite Res., **16**, 220–234, 2003

The magnetic anomaly and NRM directions of Odessa octahedrite

Minoru Funaki[1], Masami Koshita[2] and Hiroyuki Nagai[2]

[1] *National Institute of Polar Research, Kaga 1-chome, Itabashi-ku, Tokyo 173–8515*
[2] *Department of Physics, Faculties of Science, Shinshu University, Asahi 3-chome, Matsumoto 390–8621*

Abstract: The magnetic anomaly of the Odessa octahedrite (3.7 kg, a single crystal) was measured at 1, 5, 10, and 40 cm from the surface using a uniaxial fluxgate magnetometer in a μ-metal magnetic shield environment. The NRM directions of cubic subsamples were measured to take into consideration the role of the octahedron crystallography during AF demagnetization. These results indicated that the observed anomalies are strongly controlled by the shape anisotropy of the sample rather than the crystallography of the octahedrite, although weak complicated anomalies which may be related to structure appeared above 1 cm from the surface. The natural remanent magnetization of cubic subsamples was controlled by the octahedral γ (111) planes, as demagnetized directions occurred along these planes. Namely, the preferable direction of NRM is the intersection among the great circles of γ (111) crystallographic planes which are consistent with the result obtained by A. Brecher and L. Albright (J. Geomagn. Geoelectr., **29**, 379, 1977). The origin of the stable NRM component was investigated using the results of microscopic analysis, thermomagnetic curve and hysteresis parameters. Consequently, we concluded that small amounts of taenite grains and lamellae carry the stable component which is distributed along the octahedral γ (111) planes.

key word: Odessa, magnetization, magnetic field, magnetic anomaly, NRM

1. Introduction

Octahedrite characterized by Widmanstätten structure may not have any paleomagnetic meaning because of the magnetic interactions among the magnetic grains, even if it has stable natural remanent magnetization (NRM). Nevertheless, some studies have been performed to focus on the origin of the stable NRM components (*e.g.* DuBois, 1965; Brecher and Albright, 1977). These results, however, contributed to understanding not only the physical meaning of the magnetization of iron meteorites but also the basic magnetic properties of tetrataenite which is found only in meteorites. The magnetic study of iron meteorites seems relevant to estimating the magnetic signature of asteroids important to planing for the MUSES-C mission (project of the retrieve samples from a small body in the solar system and to return them to the earth). This study is considered to be a bridge between magnetic properties of iron meteorites and the magnetic signature of the iron type asteroids.

Octahedrite consisting of kamacite and taenite lathes developed along the octahedron (111) plane is often a single crystal more than several centimeters, some times

more than 1 m in size. In general, when evaluating the NRM of the octahedrite is intrinsically soft random moments, due for example to loosely pinned domain walls that align with stray fields when it was demagnetized are most characteristic. However, octahedrites occasionally carry stable NRM components (Fukuhara *et al.*, 1998; Funaki and Danon, 1998; Funaki *et al.*, 1986; Brecher and Albright, 1977). The reason has been considered due to the magnetocrystalline anisotropy (Brecher and Albright, 1977; Fukuhara *et al.*, 1998) and the high coercivity tetrataenite lamellae developed along the limbs of taenite (Funaki *et al.*, 1986). If the NRM is controlled strongly by this magnetocrystalline anisotropy, the magnetic signature of the octahedrite must be dictated by the octahedron structure.

Odessa was selected for this study. It is classified as a coarse octahedrite (Og) based on the band width of the Widmanstätten structure (1.70 ± 0.25 mm), and group I chemical composition (7.35% Ni, 0.48% Co, about 0.35% P, 0.5% S, 0.2% C), according to Buchwald (1975). Neumann bands are observed in kamacite and troilite-graphite-silicate nodules are present. Jaeger and Lipschutz (1967) estimated Odessa to be mildly shock below 13 GPa using artificially shocked Odessa specimens. Our sample is 3.7 kg in weight and about $10 \times 8 \times 8$ cm in irregular shape. The surface is overall decorated by humps and gentle depressions. Although it is covered by a black fusion crust, metallic shiny colored area appear frequently on the ridges and corners of the sample due to rubbing. Weathered products as FeOOH were not visible, by naked eyes, on the surface.

2. Sample and instruments

Several areas of the Odessa surface were polished by sand papers (#800 and #1200 grid), and subsequently etched with nital (nitric acid (10%) diluted with ethanol (90 %)) to identify the crystallization pattern referred to as the Widmanstätten structure. We confirmed that our sample is a single crystal from the analysis of the polished surface structure. One slice (5.4×4.3 cm in size with 1.6 cm in the maximum thick) was cut along a plane of the structure (octahedral γ (111)). The sliced sample was divided into 3 disk samples 0.5 cm thick along the $(\bar{1}\bar{1}\bar{1})$ plane in Fig. 1a. The cubic samples (OD-1 to OD-6) and that of OD-7 were obtained from the interior and center disks respectively with orientations, as shown in Fig. 1b. They weighed between 1.05 and 0.92 g and were cubic about 0.5 cm on edge. The samples OD-1, -2, -3, -4, -5 and -6 were at least 1.1 cm from the fusion crust, while the sample (OD-7) was located 0.5 cm from the fusion crust.

The block sample was mounted on a binary-axes rotation stage which was made of aluminum and wood (Fig. 2). The system was installed in a double-layered μ-metal magnetic shield whose residual magnetic field was reduced to less than 53 nT by means of adjusting the entrance of shield to the geomagnetic W-E direction. The coordinates of the sample were arbitrarily assigned to the axes of the rotation stage respectively as latitude and longitude. The magnetic field intensity was measured by a uniaxial fluxgate magnetometer having a resolution of 0.5 nT. The probe of the magnetometer was directed to the center of sample with 1 cm in distance from the surface through a cone-shaped wooden spacer. The field was measured at every 5° in the latitude and

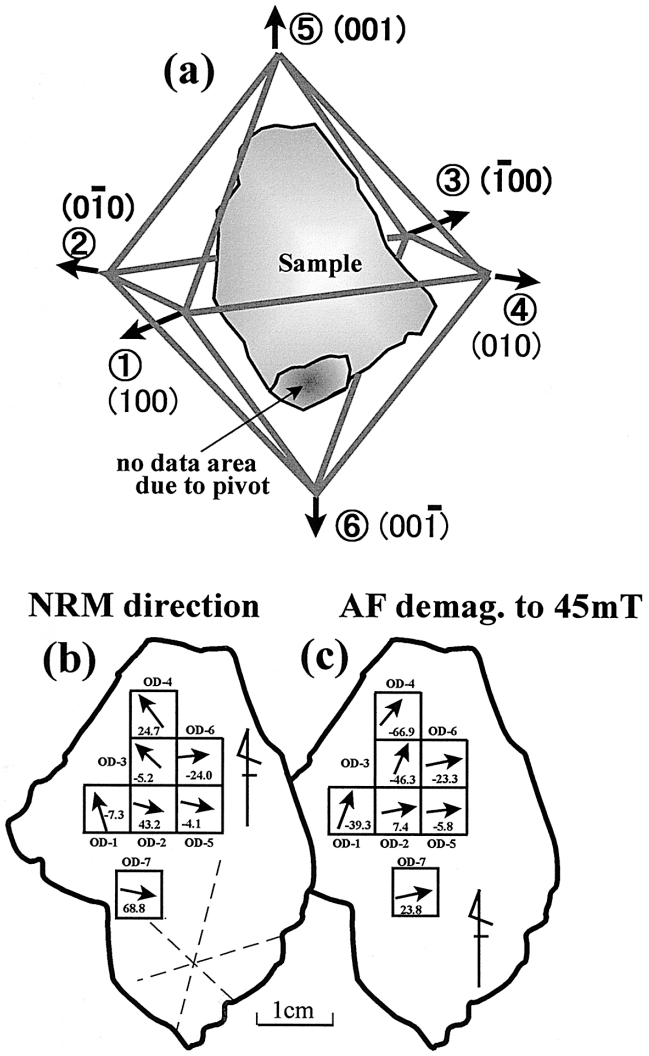

Fig. 1. (a) A sample coordinate of the bulk sample of Odessa associated with crystallography, and the crystallographic axes are denoted by ① to ⑥. (b) and (c) the coordinates of the divided samples before and after AF demagnetization to 45 mT. In figure (b) and (c), arrows denote the NRM declination with numerical value indicating inclination, and dotted lines denote the principal axes of the octahedral crystallography.

every 10° in the longitude. Distances from the center to the surface under each measurement point were recorded in order to understand the surface topography. These measurements were repeated at distances of 5, 10, and 40 cm from the surface, although the intervals of measurement were changed to every 10° in the latitude and longitude in these cases. The magnetic field could not be measured in the area between 90° and 70° and between −90° and −70° in latitude due to obstruction by the pivots. Finally the coordinate was converted to the octahedron crystallization, as shown in

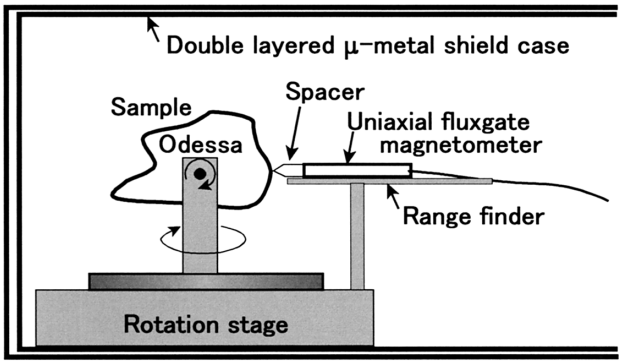

Fig. 2. An outline of the magnetic measurement setup located in the magnetic shield case.

Fig. 1a, where the directions from ① to ⑥ correspond to the octahedron crystallography (100), (0$\bar{1}$0), ($\bar{1}$00), (010), (001) and (00$\bar{1}$) respectively.

3. Magnetic anomaly

At 1 cm from the surface, magnetic field ranging from −59000 to 38100 nT could be measured for Odessa, as shown in Fig. 3. The conspicuous positive (A, B) and negative (C, D and E) anomalies were resolved. The anomalies B, C and D were

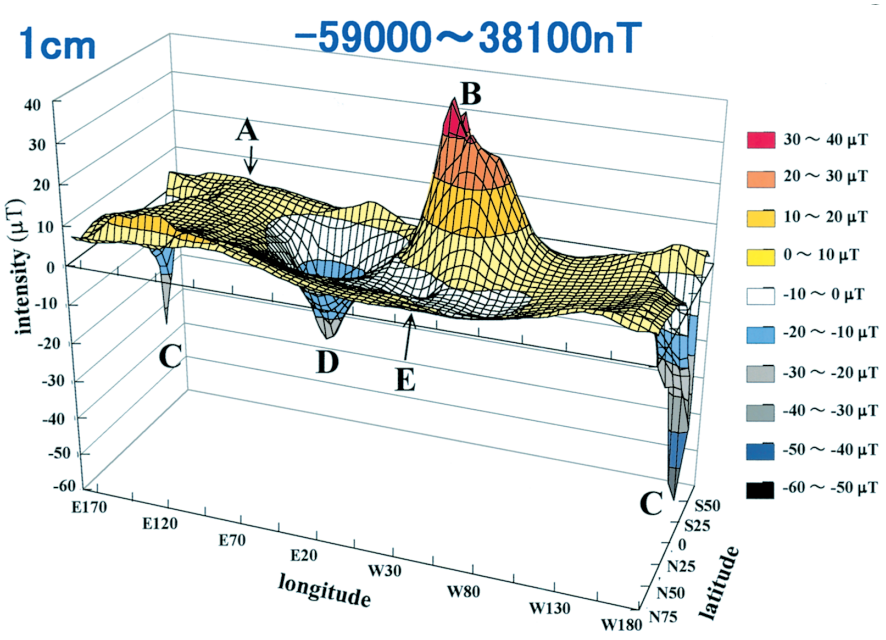

Fig. 3. A magnetic anomaly pattern between −59000 and 38100 nT measured at 1 cm from the surface. A, B, C, D and E are dominant magnetic anomalies.

prominent, sharp, and strong compared with those of A and E. Weak magnetic fields between −10 and 10μT was observed over the surface illustrating a gentle warping topology. Figure 4 outlines the octahedron crystallography and the associating mag netic anomaly pattern presented for clarity using a 10-grade color scale on the 3-dimensional sample presentation. Each view from 1 to 6 corresponds to the direction denoted in Fig. 1a. Red (blue) in color is the positive (negative) anomaly, while yellow and light red and blue are the weaker anomalies, and gray is no data due to shadow by pivots. In this figure the positive anomalies A and B and the negative ones C, D and E appeared, with the anomalies B and C being stronger than the others. The anomalies A–E are formed upon the sharped surface or at edges of the sample. They are not seen in association with the crystallographic axes, such as (100), (010), (111) for example. It may be concluded, therefore, the shape anisotropy of the sample is responsible for the magnetic anomaly pattern rather than the octahedron crystallography.

At a distance of 5 cm, the magnetic field varied from −9959 to 4244 nT. The strongest peak value (anomaly C) decreased to 16.9% compared to the 1 cm case. Anomalies A, B, C and D appear more broad and they are connected with the positive group (A and B) and negative one C and D), while anomaly E merges with C, as shown in Fig. 5.

At a distance of 10 cm, the magnetic field varied from −2.128 to 1.088 nT with much broad swing of anomalies A, B and C, while anomaly D merged with anomaly C,

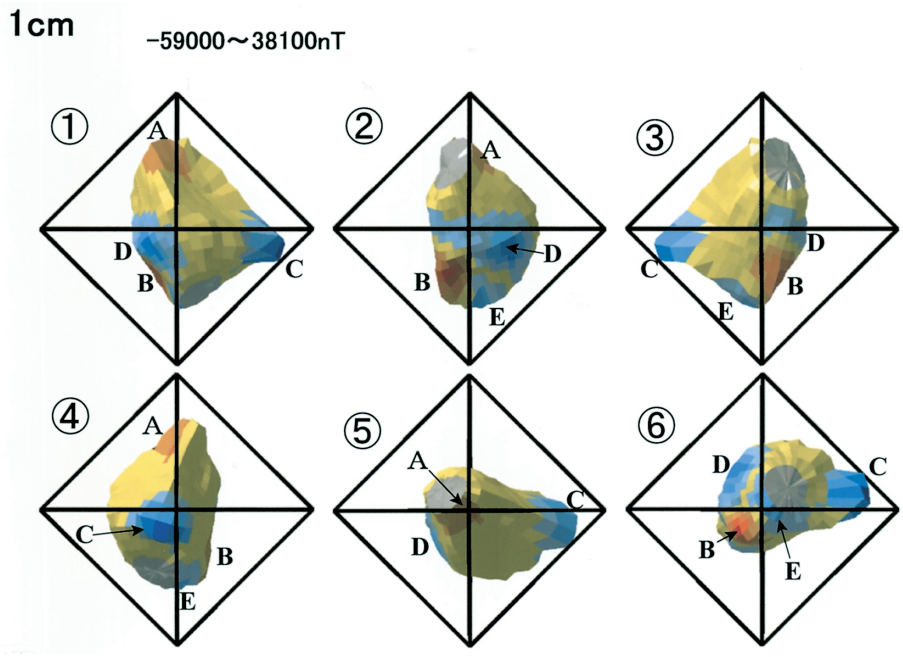

Fig. 4. A magnetic anomaly pattern describing on the sample measured at 1 cm from the surface. ① to ⑥ are the directions to see the sample from respective crystallographic axes (see Fig. 1a).

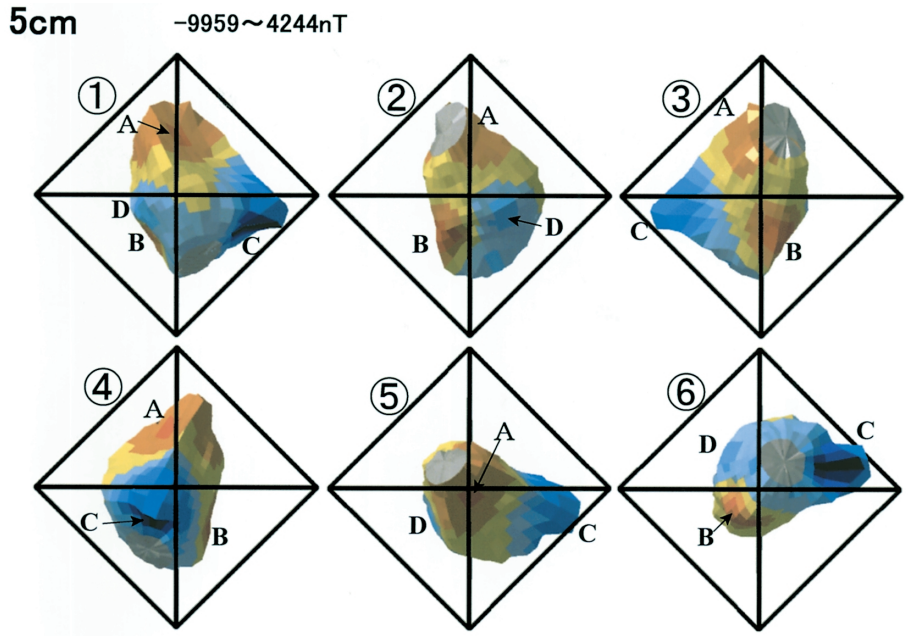

Fig. 5. Same as Fig. 4 except at 5 cm from the surface.

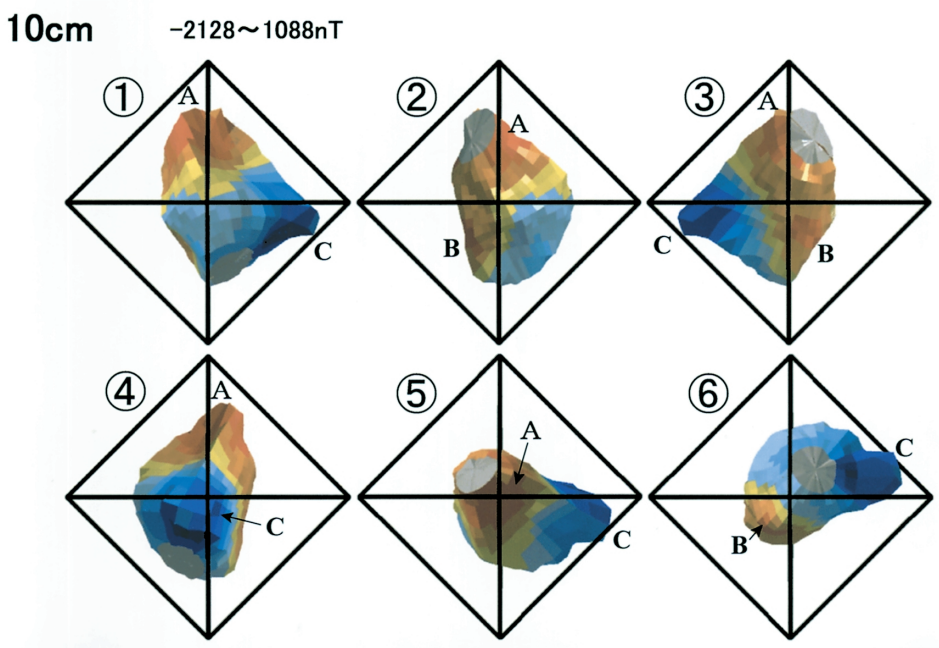

Fig. 6. Same as Fig. 4 except at 10 cm from the surface.

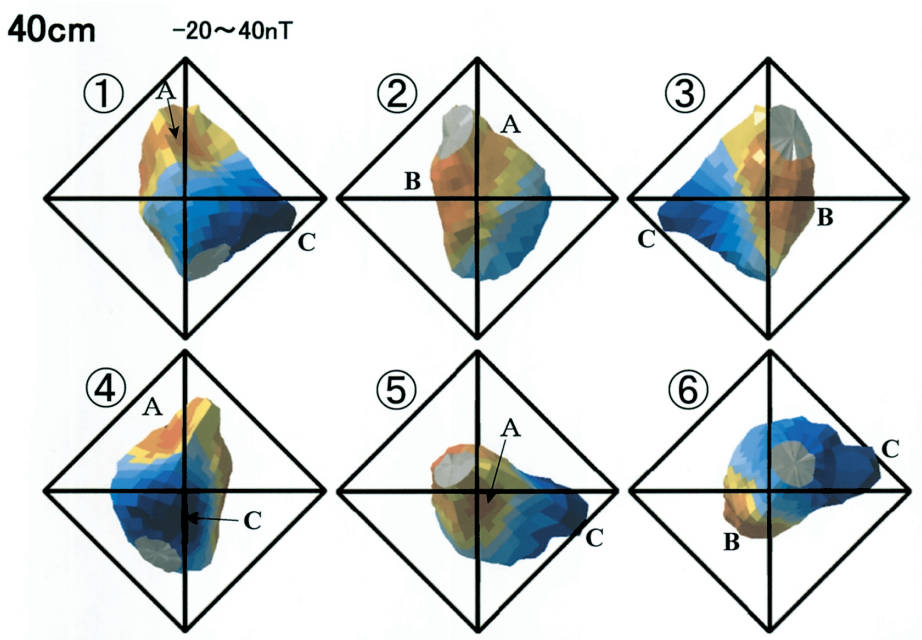

Fig. 7. Same as Fig. 4 except at 40 cm from the surface.

as shown in Fig. 6. The peak intensity of anomaly C deceased 3.6% versus that at 1 cm. These distributions of anomalies are almost similar to the dipolar pattern.

At the distance of 40 cm, the distribution pattern of the field intensity emphasized a dipolar pattern, as shown in Fig. 7. The peak values of −20 nT (anomaly C) and 40 nT (anomaly B) were less than only 0.1% versus that of 1 cm. The positive anomaly A merged with anomaly B.

4. Magnetic properties

4.1. AF demagnetization of NRM

The NRM's of every cubic sample OD-1 to OD-7 (0.24×10^{-2}–1.19×10^{-2} Am^2/kg) were measured by a spinner magnetometer (Tierra Tecnica Co. Ryoko) and were demagnetized by alternating magnetic field (AF demagnetization) up to 50 mT in steps of 5 mT using a 3-axes AF demagnetizer. Two types of demagnetization curves appeared. One is the very stable NRM without almost no unstable component (samples OD-5 and -6), while the NRM of other samples consists of stable and unstable components (samples OD-1, -2, -3, -4 and -7). Figure 8 shows the typical demagnetization curves of NRM intensity (a) and Zijderveld projection (b) of the sample OD-6 and OD-4. The variations of direction for the 7 samples are plotted in the figure (c) with the 4 great circles *(a), (b), (c)* and *(d)* of the octahedral γ (111) planes. The intensity of sample OD-6 decreased gradually and the directions did not change drastically. That of the sample OD-4 varied drastically between 0 and 10 mT and smoothly changed between 10 and 50 mT. The direction of this sample was very unstable up to 10 mT,

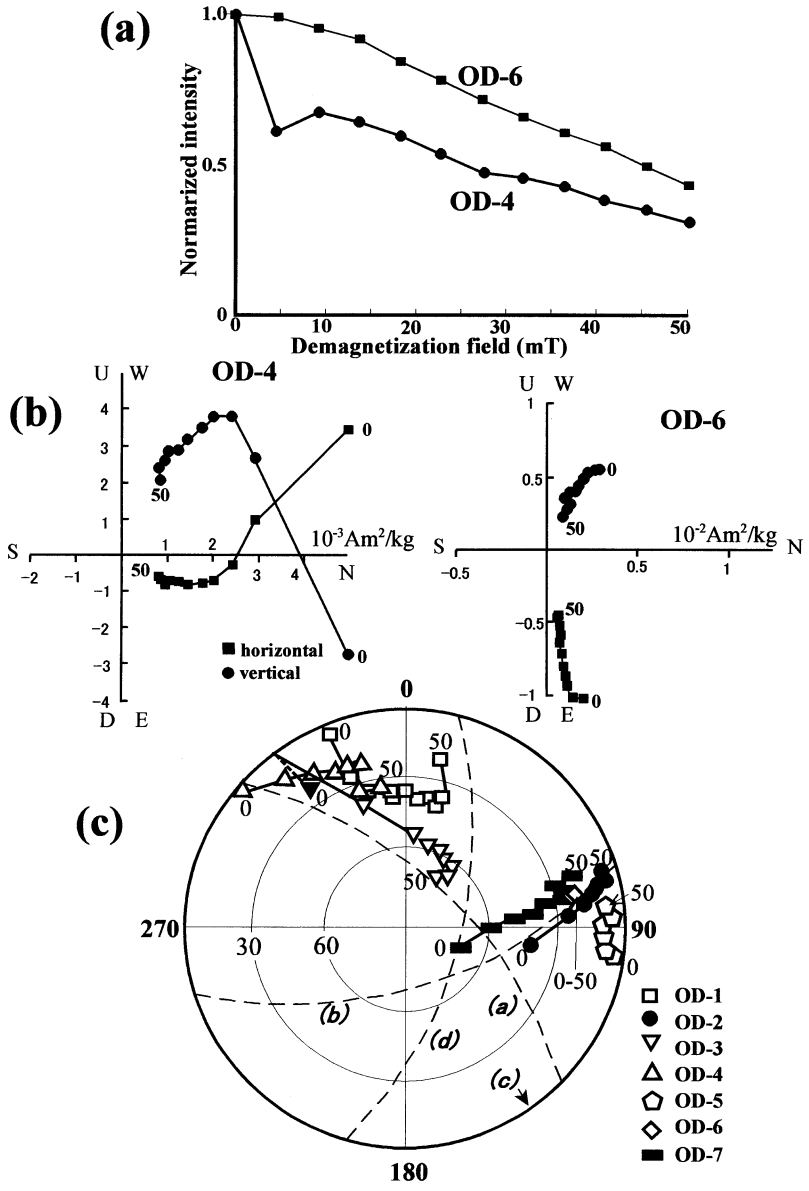

Fig. 8. AF demagnetization of NRM for the subsamples. (a) Intensity change curves, (b) Zijderveld projection, (c) directional change and indicated γ (111) crystallographic planes denoted by dashed curves.

while it was more stable between 15 and 50 mT. In general, the NRM directions of all 7 samples gradually shifted up to 15 mT, and then were more stable to 45 mT. The directions, except the sample OD-1, seem to change roughly along the 3 great circle paths; along the circle *(a)* for samples OD-3 and -4, the circle *(b)* for the samples OD-2,

-6 and -7, and the circle *(c)* for the sample OD-5, as shown in Fig. 8. The reason for deviation from a circle path for OD-1 is estimated to be an orientation error when the sample was set up in the sample holder. The small sample sizes were difficult to handle. The NRM directions of samples OD-2, -5, -6 and -7 make a cluster after AF demagnetization to 45 mT with mean direction of I=1, D=79, precision (K)=15 and 95% probability of NRM direction (α_{95})=24. Samples OD-1, -3 and -4 shifted along the other great circle, although their directions after the demagnetization scattered widely.

4.2. Anisotropy magnetic susceptibility

Anisotropy of magnetic susceptibility (AMS) of the samples OD-1 to -7 was measured at room temperature using a 2 mT alternating magnetic field (2000 Hz) by susceptibility meter KY-3 (AGICO Inc.). The AMS of individual samples is defined by the maximum (k_{max}), intermediate (k_{int}) and minimum (k_{min}) values of their principal axes of an ellipse which approximated it. Anisotropy degrees are given by the ratios of $L=k_{max}/k_{int}$ and $F=k_{int}/k_{min}$ indicating alignment of the magnetic minerals as lineation and foliation, respectively. The intensity of susceptibility of these samples ranged from (k_{min}) 3.72SI to (k_{max}) 4.54SI with the mean value (k_{mean}) 4.19SI. The degrees of these samples showed the prolate fabric anisotropy because of the ranges as L=1.01–1.08 and F=1.04–1.13. Their directions of the anisotropic principal axes and the mean directions of K_{max}, K_{int} and K_{min} are plotted in Fig. 9 associated with an ellipse of the 95% probability (κ_{95}=40) for the K_{max} and the great circle *(a), (b), (c)* and *(d)* of the octahedral (111) planes. The directions of k_{max} make a broad cluster around K_{max} (I=42, D=58) while those of k_{int} and k_{min} values distributed to almost random, suggesting the anisotropy fabric of the uniaxial prolate. The direction of K_{max} does not overlay the great circles, but it is similar to that of the γ(111) axis.

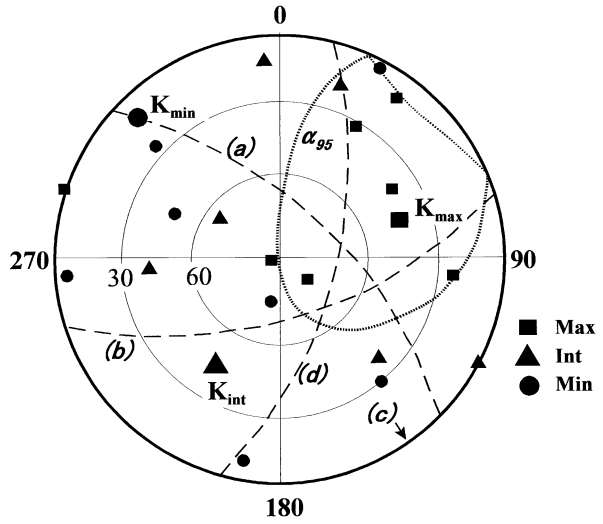

Fig. 9. Anisotropy of magnetic susceptibility (AMS) of the divided samples.

4.3. *Hysteresis and thermomagnetic properties*

Magnetic hysteresis curves were measured at room temperature in magnetic fields between 1.0 and −1.0 T using a vibrating sample magnetometer (assembled by National Institute of Polar Research, Tokyo). The saturation magnetization (I_S), saturation remanent magnetization (I_R), coercive force (H_C) and remanent coercive force (H_{RC}) were obtained from the curve, as shown in Table 1. From the value of $I_S=204.4$ Am^2/kg, kamacite is presumed to be the main mineral composition of Odessa, because this value is comparable with that of the pure iron ($I_S=217.7\,Am^2/kg$). The small value of $H_C=0.2$ mT and moderate $H_{RC}=11.8$ mT and the ratios of $I_R/I_S=5.6\times10^{-4}$ and $H_{RC}/H_C=59$ may indicate that the negligibly small amount of fine magnetic grains coexist with the large amount of low cercivity minerals.

The thermomagnetic (I_S-T) curve was measured by the vibrating sample magnetometer between room temperature and 850°C under vacuum conditions (10^{-3}Pa) in a steady magnetic field of 1.0 T, as shown in Fig. 10. The I_S-T curve indicated the phase transition from kamacite to taenite ($\alpha\rightarrow\gamma$ phase) at 740°C in the heating curve and $\gamma\rightarrow\alpha$ phase at 570°C in the cooling curve. Even if other magnetic minerals, such as taenite, are included in the sample, the saturation magnetization of these minerals seems to be negligibly small compared with kamacite and they did not appear in the I_s-T curve.

Table 1. Hysteresis properties of Odessa.

	NRM	I_S	I_R	H_C	H_{RC}	NRN/I_R
This study	0.61	204.4	0.116	0.2	11.8	0.05
Fukuhara *et al.* (1998)	3.47–3.33	149	0.610	0.83		
Unit	10^{-2} Am^2/kg	Am^2/kg	Am^2/kg	mT	mT	

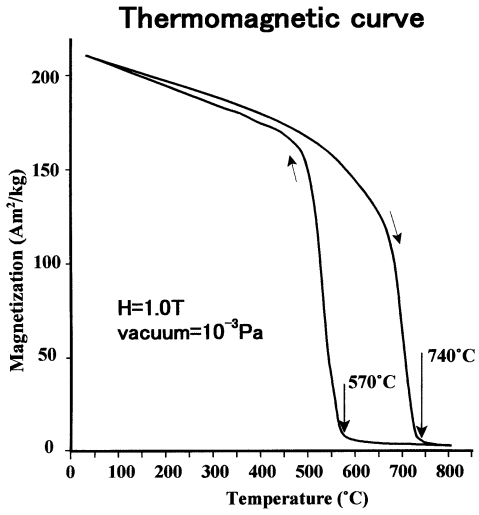

Fig. 10. Thermomagnetic curve of the 1st run cycle (10^{-3} Pa of vacuum condition) in 1.0 T of the external magnetic field.

5. Microscopic observation

A part of the interior sample was polished using 1 μm diamond paste and then it was polished by 1/4 μm silica colloid in order to remove the strain layers resulting from the polishing. Subsequently, it was etched with nital (10% nitrous and 90% ethanol). The surface was then painted by water-based super-paramagnetic magnetite of magnetic fluid (Bitter pattern). Figure 11 shows the Bitter pattern configurations of the representative field of kamacite (a) and troilite (b). In the photo (a), the magnetic fluid accumulated strongly, on a taenite grain (T1) in the plessite field, as visible dark spots and weakly on a limb of taenite lamella (T2). Typical MD structure appeared on the kamacite under the higher magnification, although it cannot be seen in this photo. Neumann lines are visible in the kamacite (K) field. In photo (b), the typical MD pattern of schreibersite (Sch; $(Fe, Ni, Co)_3 P$) as reported by DuBois (1965) appeared

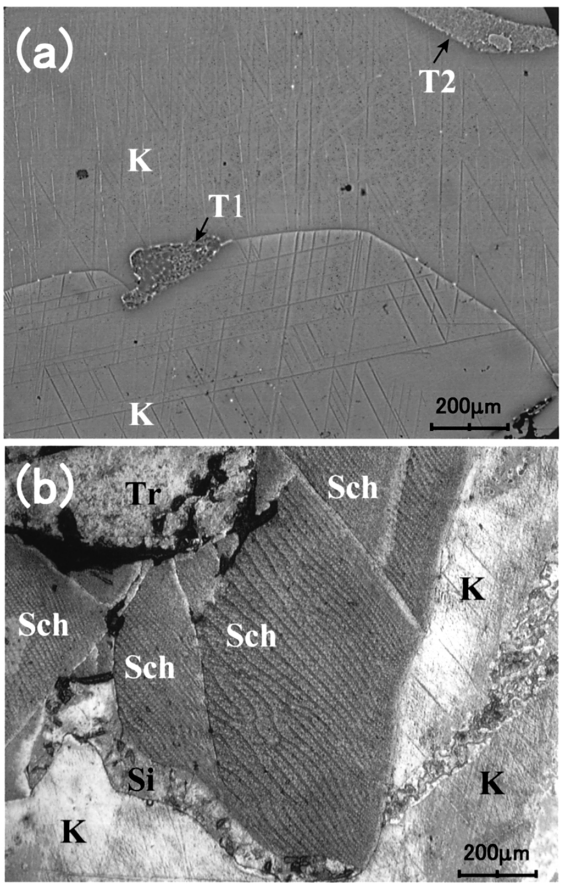

Fig. 11. A magnetic domain structure son the polished surface applied by magnetic fluid (Bitter pattern). (a) Field of view mainly kamacite (K) with minor taenite (T1, T2), (b) field of view is schreibersite (Sch), troilite (Tr: upper left) and kamacite.

along the boundary of troilite (Tr).

6. Discussions

The magnetic minerals in Odessa were investigated, using the Bitter pattern technique to identify kamacite and schreibersite, by DuBois (1965) and to identify kamacite and taenite, by Brecher and Cutrera (1976), using both Bitter patterns and scanning electron microscope (SEM) techniques. We confirmed kamacite, taenite and schreibersite magnetic minerals of in Odessa by Bitter patterns in this study. Since schreibersite is only formed along the limbs of troilite inclusion, the latter authors might not have observed it since they viewed the pure FeNi region. The I_S-T curve in Fig. 10 showed the typical curve of kamacite with 7 wt%Ni, as a phase transition from α- to γ-phase ($\alpha \rightarrow \gamma$) at 740°C in the heating curve and $\gamma \rightarrow \alpha$ at 570°C in the cooling curve. This result supports 7.35% Ni bulk composition in Odessa reported by Buchwald (1975). However, there is no Curie point of taenite and schreibersite (310°C; Lovering and Parry, 1962) in the curve in spite of the results of Bitter pattern analysis. As the saturation magnetization $I_S = 204.4\ Am^2/kg$ is consistent with that of the pure Fe 93% Ni 7%, no identification of taenite and schreibersite in the I_S-T curve probably indicates the distribution of these minerals is heterogeneous.

Brecher and Albright (1977) during AF demagnetization showed a very unstable NRM up to 2.5 mT characterized by a rapid decrease in intensity and drastic shift of the direction, with improved behavior between 2.5 and 30 mT. Fukuhara *et al.* (1998) reported a stable NRM component which was demagnetized at 580°C while decaying 60–80% by 300–400°C during thermal demagnetization. If the NRM originated due artificial contamination by strong magnets, the ratio of NRM/I_R should be larger than 0.01 (Wasilewski and Dickinson, 1998). As the ratio of our sample is not large than 0.05, the samples were likely not affected strongly by artificial contaminations. According to Buchwald (1975), the maximum temperatures experienced the atmosphere by typical iron meteorites are estimated to be more than 1500°C at the fusion crust, 750°C at 2.5 mm depth and 300–400°C at 10 mm depth from the surface. The sample OD-7, 0.5 mm from the fusion crust, should be heated to less than 750°C, suggesting TRM acquisition in the earth's magnetic field below 580°C, the NRM blocking temperature (Fukuhara *et al.*, 1998). Probably the stable NRM component might reflect the thermoremanent magnetization (TRM). If the TRM is acquired after landing on the earth, the NRM of the sample near the fusion crust (OD-7) would be magnetized on the earth and that of the most interior sample (OD-2) may still suffer minor thermal influence. The characteristics of the NRM of both samples are not so different each other as we observed the NRM intensity and directional change before and after AF demagnetization (Fig 1b,c). There is no evidences of TRM acquisition in the earth's magnetic field for our sample. The most plausible explanation of the NRM characteristics is that our samples OD-1 to -7 were not heated by TRM because of newly formed samples being the result of a fragmentation of a larger body near the earth's surface. DuBois (1965) studied the NRM directions of Odessa collected from the Odessa Crater (Odessa, Texas). His results showed that the magnetization of Odessa meteorites was not parallel to the earth's magnetic field at the sampling sites suggesting no remagnetiza-

tion after landing on the earth. From these viewpoints, we consider the interior more than 5 mm beneath the fusion crust of the Odessa samples did not acquirer TRM by atmosphere heating.

The stable NRM component seems to be carried by taenite because of following aspects: (1) the NRM was demagnetized before 580°C which consists with a Curie point of taenite with Fe 50% Ni 50%. If kamacite carries it, a part of NRM may be survived around the $\alpha \rightarrow \gamma$ phase transition at 740°C. (2) Strong accumulation of magnetic fluid like grape-clusters appeared on taenite grains in plessite and on taenite lamellae, while the typical MD structures appeared on kamacite and schreibersite. (3) The small $H_C = 0.2$ mT and relatively large $H_{RC} = 11.8$ mT values imply the MD structure for the main magnetic minerals associated with very small amounts of fine-grained ones (single-domain (SD) or pseudosingle-domain (PSD) grains). Kamacite is the most abundant magnetic mineral, but taenite and schreibersite are extremely minor abundant as observed by the microscope and I_S-T analyses. It can be concluded, therefore, that the stable NRM component is carried by taenite, while the unstable component might be carried by kamacite and schreibersite.

The magnetization direction in octahedrites appears to be preferentially associated with the octahedral γ (111) crystallographic planes on which α (110) plates nucleated and grew, and/or aligned with their intersections, whose intersections define "magnetic easy axes" (Brecher and Albright, 1977). The magnetization of the samples OD-2 to -7 roughly aligned the directions along the 3 great circles during AF demagnetization, as regulated the octahedral γ (111) planes. The samples OD-2, -5, -6 and -7 made a cluster at I = 1 and D = 79 which is consistent with the intersection between the circle (b) and (c). The magnetization of the sample OD-4 is also stabilized around the intersection of the circles (a) and (d). These distributions of NRM directions indicate that the preferable direction of NRM is the intersection among the great circles of γ (111) crystallographic planes. These results are essentially consistent with the NRM distribution obtained by Brecher and Albright (1977). From these viewpoints, we concluded that the NRM direction of Odessa is regulated by the distribution of taenite grains and lamellae developed along the γ (111) planes of Widmanstätten structure. When Odessa is located in a magnetic field, the induced magnetization must be considered. As the AMS value derives from the abundance of the low coercivity minerals, kamacite influenced the AMS strongly for Odessa.

The induced magnetization is proportionate to the applied field in the range of several mT. The NRM intensity $R = 0.61 \times 10^{-2}$ Am^2/kg is converted to 48.8 A/m, assuming density of $\rho = 8$ for Odessa. As the residual magnetic field in the μ-metal shield case is less than 53 nT, the maximum induced magnetization is driven to 2.22×10^{-7} A/m from susceptibility $K_{mean} = 4.19$ (SI). Therefore, it is negligibly small compared with NRM intensity. Consequently we concluded that the magnetic anomaly patterns in Fig. 3–7 are due to the remanent magnetization of Odessa.

The magnetic anomaly pattern observed at 1 cm from the surface yielded a complicated distribution not only in intensity (Fig. 3) but also in direction (Fig. 4). Such a distribution, if anything, implies that the sample cannot record the magnetization which was acquired in a uniform magnetic field. As Odessa has magnetic easiest planes and easiest axes as discussed above, the complicated distribution of directions is

explained by these crystallographic characteristics. However, the larger magnetic anomalies appear at humps and corners of the sample, and weaker anomalies were located at the relatively flat surface. When the distance of measurement is farther from the surface, the anomalies seem to be strongly affected by shape anisotropy of the sample. Weak anomalies are merged with the strongest positive and negative anomalies, showing the dipole field, at 40 cm from the surface as would be expected. Wasilewski *et al.* (1997) observed the dipole magnetic field on Canyon Diablo (coarse octahedrite). The dipole field might be obtained due to enough distances from the surface, otherwise more complicated anomaly patterns should be obtained.

7. Conclusion

Odessa consists of mainly kamacite associated with a small amount of taenite and schreibersite. Stable NRM appears to be carried by taenite grains and lamellae that are developed along the Widmanstätten structure. The single crystal of Odessa sample showed complicated magnetic anomalies 1 cm from the surface, but it showed almost dipole magnetization at 40 cm from the surface. Probably one of the reasons of the complicated anomalies is due to the magnetic easiest axes. Although the anomalies are regulated by the shape anisotropy and alignments of the octahedral γ (111) planes, the former is much stronger than the latter. Consequently, the dipole magnetization is dominant when the measured distance increases from the surface. The magnetization of divided samples is demagnetized along the great circles of γ (111) crystallographic planes. The most stable NRM directions appears to be regulated by the intersection among the great circles. However, if Odessa is located in the magnetic field, the magnetization would be influenced strongly by the induced magnetization due to dominant kamacite.

Acknowledgments

The authors wish to express their appreciation to Dr. P. Wasilewski (Goddard Space Flight Center, NASA) for useful suggestions in this paper.

References

Bachwald, V.F. (1975): Handbook of Iron Meteorites, vol. 1. Los Angeles, Univ. California Press, 52 p.

Brecher, A. and Albright, L. (1977): The thermoremanence hypothesis and the origin of magnetization in iron meteorites. J. Geomagn. Geoelectr., **29**, 379–400.

Brecher, A. and Cutrera, M. (1976): A scanning electron microscope (SEM) study of the magnetic domain structure of iron meteorites and their synthetic analogues. J. Geomagn. Geoelectr., **28**, 31–45.

DuBois R.L. (1965): Some investigations of remanent magnetism and domain structures of iron meteorites. J. Geomagn. Geoelect., **17**, 3–4, 381–390.

Fukuhara, T., Funaki, M. and Nagai, H. (1998): Magnetic contaminations of small iron meteorites, Odessa and Gibeon. Antarct. Meteorites Res., **11**, 178–188.

Funaki, M. and Danon, J. (1998): Characteristics of natural remanent magnetization of Nova Petrópolis iron meteorite (II). Antarct. Meteorites Res., **11**, 189–201.

Funaki, M., Nagata, T. and Danon, J.A. (1986): Magnetic properties of lamellar tetrataenite in Toluca iron meteorite. Mem. Natl Inst. Polar Res., Spec. Issue, **41**, 382–393.

Funaki, M., Taguchi, I. Danon, J., Nagata, T. and Kondo, Y. (1988): Magnetic and metallographical studies of the Bocaiuva iron meteorite. Proc. NIPR Symp. Antarct. Meteorites, **1**, 231–246.

Jaeger, R.R. and Lipschutz, M.E. (1967): Implications of shock effects in iron meteorites. Geochim. Cosmochim. Acta, **31**, 1811–1832.

Lovering, J.F. and Parry, L.G. (1962): Thermomagnetic analysis of co-existing nickel-iron metal phases in iron meteorites and the thermal histories of the meteorites. Geochim. Cosmochim. Acta, **26**, 362–382.

Wasilewski, P.J., Dickinson, T.L, Connerney, J.E. and Funaki, M. (1987): Asteroid magnetic records - possible insight from the analysis of large meteorites. Papers presented to the 12th Symposium on Antarctic meteorites, June 8–10, 1987. Tokyo, Natl Inst. Polar Res., 203–205.

(Received October 8, 2002; Revised manuscript accepted February 13, 2003)